Synthesis of High-Surface-Area Alumina Using Aluminum Tri-*sec*-butoxide−2,4-Pentanedione−2-Propanol−Nitric Acid Precursors

L. Ji,[†,‡] J. Lin,[†] K. L. Tan,[†] and H. C. Zeng*[,‡]

Department of Physics, Faculty of Science, and Department of Chemical and Environmental Engineering, Faculty of Engineering, National University of Singapore, 10 Kent Ridge Crescent, Singapore 119260

Received June 29, 1999. Revised Manuscript Received October 26, 1999

Transparent alumina gels have been prepared with a simple precursor system, aluminum tri-*sec*-butoxide−2,4-pentanedione−2-propanol−nitric acid, at optimal acacH/ASB mole ratios of 0.3−0.4. The specific surface areas (S_{BET}) of the prepared gels are in the range 552−560 m^2/g after calcination at 400 °C for 2 h. It is found that the as-prepared xerogels convert into γ-Al_2O_3 at 400−800 °C and then to α-Al_2O_3 at 1000−1050 °C. Two successive changes in S_{BET} are observed in the gel phase transformations. Microporous alumina with a pore size < 16 Å can be prepared at calcination temperatures of 200−300 °C (S_{BET} = 674 m^2/g) while mesoporous alumina materials with uniform pore sizes of 29−74 Å can be obtained at 400−1000 °C using the same starting xerogel. On the basis of a large set of gelation data, it is believed that the hydrolysis of the alkoxides takes place before the condensation. The causes for the observed gel transparency and for the generation of high surface areas are also discussed on the basis of the results of synthesis experiments and the findings of XRD/FTIR/DTA/TGA/BET/BJH investigations.

Introduction

The synthesis of pure alumina materials via organic or inorganic sol−gel routes has been extensively studied over the past three decades due to the great technological importance of the materials and the great flexibility of the low-temperature synthetic techniques.[1−20]

In the organometallic sol−gel approach, aluminum alkoxides such as aluminum isopropoxide and aluminum *sec*-butoxide are often used for the precursor preparation. Although details for the prevailing synthesis processes vary, the methods can be broadly divided into two types. The first type, which was developed in the 1970s, involves hydrolysis of aluminum alkoxides in excess water and subsequent peptization/acidification in acid solutions.[1−4] Various alumina gels including transparent monolithic glass and aerogels have been prepared by these methods.[1−9] The second type of method, which utilizes chelating agents and aims at the control of the hydrolysis and condensation rates, also shows great flexibility in tailor-making alumina materials with desired physicochemical properties.[10−20] In particular, chelating agents such as acetylacetone, ethylacetoacetate, monoethanolamine, diethanolamine, triethanolamine, acetic acid, and long-chain carboxylic acids have been used in the modification of the chemical reactivity of the precursor compounds.[10−17] It should be mentioned that the chelating agents not only control the rates of hydrolysis and condensation but also determine the final properties of the alumina materials. Chemical reactions between the metal cations and complexing agents are expected during the synthesis and postsynthesis thermal treatments. For example, surfactant effects of ethyl acetoacetate and long-chain carboxylic acids have been recognized in the synthesis of pure

* To whom correspondence should be addressed. Telephone: +65 874 2896. Telefax: +65 779 1936. E-mail: chezhc@nus.edu.sg.
† Department of Physics, Faculty of Science.
‡ Department of Chemical and Environmental Engineering, Faculty of Engineering.

(1) Yoldas, B. E. *J. Appl. Chem. Biotechnol.* **1973**, *23*, 803.
(2) Yoldas, B. E. *J. Mater. Sci.* **1975**, *10*, 1856.
(3) Yoldas, B. E. *Am. Ceram. Soc. Bull.* **1975**, *54*, 286.
(4) Yoldas, B. E. *Am. Ceram. Soc. Bull.* **1975**, *54*, 289.
(5) Chane-Ching, J.-Y.; Klein, L. C. *J. Am. Ceram. Soc.* **1988**, *71*, 83.
(6) Chane-Ching, J.-Y.; Klein, L. C. *J. Am. Ceram. Soc.* **1988**, *71*, 86.
(7) Assih, T.; Ayral, A.; Abenoza, M.; Phalippou, J. *J. Mater. Sci.* **1988**, *23*, 3326.
(8) Oh, C.-S.; Tomandl, G.; Lee, M.-H.; Choi, S.-C. *J. Mater. Sci.* **1996**, *31*, 5321.
(9) Janosovits, U.; Ziegler, G.; Scharf, U.; Wokaun, A. *J. Non-Cryst. Solids* **1997**, *210*, 1.
(10) Babonneau, F.; Coury, L.; Livage, J. *J. Non-Cryst. Solids* **1990**, *121*, 153.
(11) Nass, R.; Schmidt, H. *J. Non-Cryst. Solids* **1990**, *121*, 329.
(12) Elaloui, E.; Pierre, A. C.; Pajonk, G. M. *J. Catal.* **1997**, *166*, 340.
(13) Tadanaga, K.; Ito, S.; Minami, T.; Tohge, N. *J. Non-Cryst. Solids* **1996**, *201*, 231.
(14) Ayral, A.; Phalippou, J.; Droguet, J. C. *Better Ceramics through Chemistry III*; Materials Research Society Symposium Proceedings Vol. 121; Materials Research Society: Pittsburgh, PA, 1988; p 239.
(15) Rezgui, S.; Gates, B. C. *Chem. Mater.* **1994**, *6*, 2386.
(16) Rezgui, S.; Gates, B. C.; Burkett, S. L.; Davis, M. E. *Chem. Mater.* **1994**, *6*, 2390.
(17) Vaudry, F.; Khodabandeh, S.; Davis, M. E. *Chem. Mater.* **1996**, *8*, 1451.
(18) Kurokawa, Y.; Shirakawa, T.; Saito, S.; Yui, N. *J. Mater. Sci. Lett.* **1986**, *5*, 1070.
(19) Ray, J.; Chatterjee, M.; Ganguli, D. *J. Mater. Sci. Lett.* **1993**, *12*, 1755.
(20) Ramanathan, S.; Roy, S. K.; Bhat, R.; Upadhyaya, D. D.; Biswas, A. R. *J. Alloys Compd.* **1996**, *243*, 39.

10.1021/cm990404u CCC: $19.00
Published on Web 03/24/2000

alumina mesoporous materials.[11,17] The effects of chelating agents on the specific surface area, the pore size distribution, and the morphology of alumina materials have been investigated in certain systems.[11−17] It is known that, for most cases, the synthesis parameters are interrelated. For instance, with small variations in the process sequence, the starting material concentrations, and the postsynthesis treatments, the above textural properties can be significantly different, owing to the complex chemistry of these materials.[15−17]

As part of our recent effort in the synthesis of catalytic materials,[21−25] in this paper we report an investigation of the synthesis of high-surface-area alumina using a relatively simple precursor system: aluminum trisec-butoxide−2,4-pentanedione (acetylacetone)−2-propanol−nitric acid. A common chelating agent, acetylacetone, was chosen here in order to reduce the complexity of the reactions. By conducting a wide range of synthetic experiments and materials characterization, we have been able to identify the key parameters for this precursor system. In addition, the present work also looks into the fundamental aspects of the synthesis regarding hydrolysis, condensation, acidification, and possible reasons for the high-surface-area formation.

Experimental Section

Sample Preparations. Alumina xerogels were prepared by hydrolysis and polycondensation of aluminum tri-*sec*-butoxide (Al(O-*s*-Bu)$_3$ or ASB) in 2-propanol (*i*-PrOH) solvent with 2,4-pentanedione (acetylacetone, or acacH, and $C_5H_8O_2$) as chelating agent and nitric acid (HNO_3) as acidification agent. The chemicals used in the present work were ASB (Aldrich, 97%), *i*-PrOH (Merck, 99.7%), acacH (Fluka, >98%), and HNO_3 (Merck, 65%). Compositions for various precursor solutions for gel synthesis are detailed in Table 1. In a premixing step, precursor solutions were prepared by dissolving 10 mmol of ASB into 0−400 mmol of *i*-PrOH together with 0−8 mmol of acacH under magnetic stirring. After mixing for 30 min, hydrolysis was then started by adding 0.2−0.8 mL of HNO_3 solution (noting the low molarity *M* in Table 1) or 0.1−0.6 mL of deionized water dropwise to the solutions. The resulting solutions (yellowish) were then covered (i.e., sealed) and stirred vigorously until gelation occurred, which was followed by a 10-day static aging at room temperature. The aged gels were dried in air under ambient conditions for another 10 days.

To study the thermal behavior and phase transformations, the above-prepared xerogels were calcined in alumina crucibles in an air atmosphere under static conditions in a muffle furnace. The temperature was raised at a rate of 5 °C/min (the same was used in the cooling) to a desired temperature (in the range 200−1200 °C with an increment of 100 °C) and kept at the same temperature for 2 h before cooling. The calcined products were yellowish when heat-treated at 200 and 300 °C and whitish if treated at higher temperatures.

Sample Characterization. Structural phase analysis with the X-ray diffraction (XRD) method was performed on crushed xerogels in a Shimadzu XRD-6000 X-ray diffractometer using Cu Kα radiation ($\lambda = 1.5418$ Å). A continuous scan mode was used to collect 2θ data from 10° to 80° with a 0.02° sampling pitch at a scanning speed of 5°/min.

Chemical bonding information on metal−oxygen, organic compounds, and functional groups were investigated with Fourier transform infrared spectroscopy (FTIR, Perkin-Elmer 2000) using the potassium bromide (KBr) pellet technique; each spectrum was collected after 32 scans for the wavenumber range 400−4000 cm^{-1} at a resolution of 4 cm^{-1}.

To understand the thermal behaviors of the xerogels, investigations with differential thermal analysis (DTA, Perkin-Elmer DTA 7 Series UNIX V 4.0) and thermogravimetric analysis (TGA, Perkin-Elmer TGA 7 Series BTW) were conducted. In the DTA/TGA study, 20 mg of sample was heated at a scanning rate of 10 °C/min in an air atmosphere (the gas flow rate: 40 mL/min).

Full adsorption−desorption isotherms of nitrogen at 77 K on all calcined xerogels were measured at various partial pressures in a Quantachrome NOVA-1000 apparatus. Specific surface areas (S_{BET}s) and pore-size distributions (PSDs) were determined with the Brunauer−Emmett−Teller (BET) method and the Barret−Joyner−Hallender (BJH) method, respectively. BET surface areas were obtained from six adsorption data points in the relative pressure ($P/P°$) range 0.02 to 0.30 whereas the PSDs were derived from the desorption isotherms. Before the BET/BJH measurements, all samples were degassed for 3 h at a temperature slightly below the calcination temperature or below 350 °C.

Table 1. Chemical Compositions and Sample Nomenclature for Xerogel Samples

sample	PrOH (mmol)	acacH (mmol)	ASB (mmol)	HNO_3 (mL)	H_2O (mL)
A1	0	3.5	10	0.5 (0.5 M)	
A2	50	3.5	10	0.5 (0.5 M)	
A3	100	3.5	10	0.5 (0.5 M)	
A4	150	3.5	10	0.5 (0.5 M)	
A5	200	3.5	10	0.5 (0.5 M)	
A6	250	3.5	10	0.5 (0.5 M)	
A7	300	3.5	10	0.5 (0.5 M)	
A8	350	3.5	10	0.5 (0.5 M)	
A9	400	3.5	10	0.5 (0.5 M)	
B1	150	0	10	0.5 (0.5 M)	
B2	150	1	10	0.5 (0.5 M)	
B3	150	2	10	0.5 (0.5 M)	
B4	150	3	10	0.5 (0.5 M)	
B5	150	4	10	0.5 (0.5 M)	
B6	150	5	10	0.5 (0.5 M)	
B7	150	6	10	0.5 (0.5 M)	
B8	150	7	10	0.5 (0.5 M)	
B9	150	8	10	0.5 (0.5 M)	
C1	150	3.5	10	0.5 (0.1 M)	
C2	150	3.5	10	0.5 (0.2 M)	
C3	150	3.5	10	0.5 (0.4 M)	
C4	150	3.5	10	0.5 (0.5 M)	
C5	150	3.5	10	0.5 (0.6 M)	
C6	150	3.5	10	0.5 (0.8 M)	
C7	150	3.5	10	0.5 (1.0 M)	
C8	150	3.5	10	0.5 (1.2 M)	
C9	150	3.5	10	0.5 (1.5 M)	
C10	150	3.5	10	0.5 (2.0 M)	
D1	150	3.5	10	0.2 (0.5 M)	
D2	150	3.5	10	0.4 (0.5 M)	
D3	150	3.5	10	0.5 (0.5 M)	
D4	150	3.5	10	0.6 (0.5 M)	
D5	150	3.5	10	0.8 (0.5 M)	
E1	150	3.5	10		0.1
E2	150	3.5	10		0.2
E3	150	3.5	10		0.3
E4	150	3.5	10		0.4
E5	150	3.5	10		0.5
E6	150	3.5	10		0.6
F1	150	3.5	10	0.5 (0.5 M)[a]	
F2	150	3.5	10	0.5 (0.5 M)[b]	
G1	150	3.5	10[c]	0.5 (0.5 M)	
G2	150	0	10[c]	0.5 (0.5 M)	

[a] 0.5 M $NH_3 \cdot H_2O$ solution. [b] 0.5 M NaOH solution. [c] 10 mmol of $Al(NO_3)_3 \cdot 9H_2O$.

(21) Xu, Z. P.; Zeng, H. C. *J. Mater. Chem.* **1998**, *8*, 2499.
(22) Zeng, H. C. *Inorg. Chem.* **1998**, *37*, 1967.
(23) Zeng, H. C.; Sheu, C. W.; Hia, H. C. *Chem. Mater.* **1998**, *10*, 974.
(24) Zeng, H. C.; Xu, Z. P.; Qian, M. *Chem. Mater.* **1998**, *10*, 2277.
(25) Xu, Z. P.; Zeng, H. C. *Chem. Mater.* **1999**, *11*, 67.

Results

Formation of Gels. To investigate the effect of solvent on gel formation, the PrOH/ASB mole ratio was varied in the range 0−40 (samples A1−A9, Table 1), while the acacH/ASB mole ratio was kept constant at 0.35. Without PrOH solvent, white precipitates in the gel appear immediately when nitric acid solution is added to the ASB (sample A1). With the PrOH solvent, transparent gels can be prepared immediately after addition of nitric acid solution if the PrOH/ASB mole ratio is in the range 5−20 (samples A2−A5). When the precursor sols are further diluted, however, a longer gelation time is required. For example, it takes 4 days to form transparent gels for the precursor sols with a PrOH/ASB ratio of 25−30 (samples A6 and A7). If the PrOH/ASB ratio exceeds 35, no gelation is observed (samples A8 and A9) within the study period of one month. It is worthwhile noting that when $Al(O\text{-}s\text{-}Bu)_3$ is dissolved into 2-propanol, there might be an OR group exchange reaction between the O-*s*-Bu in ASB and the O-*i*-Pr in the solvent. Nonetheless, as the current work is focused on gel formation, further investigation of this aspect (solution) was not pursued.

The effect of the chelating agent acacH on gel formation was investigated in the sample series B1−B9 (Table 1). It is found that white precipitates form immediately when the acacH/ASB mole ratio is in the range 0−0.2, whereas transparent gels can be obtained soon after the nitric acid is added if the acacH/ASB ratio is in the range 0.3−0.4 (samples B4 and B5). For the syntheses with a higher acacH/ASB mole ratio (e.g., samples B6−B9), gelation does not occur. Instead, small needle-shaped crystallites can be seen in the bottom of the transparent sols of B8 and B9.

Experiments C1−C10, D1−D5, and E1−E6 (Table 1) were designed to examine the effects of acidity and water on gelation reactions. It was observed that, with an increase in HNO_3 acidity (C1−C10), transparent gels can still be obtained until a critical acid concentration. For example, gelation times in the high-acidity cases C9 and C10 are extremely short and the prepared gels are whitely opaque. The gelation rate in D1 is very slow because the amount of nitric acid (and thus water, 0.2 mL) is too low. When the amount of the acid is increased (0.4−0.8 mL, D2−D5), rapid gelation is observed and the resultant gels are transparent. When deionized water is used instead of nitric acid, as studied in E1−E6 (Table 1), immediate gelation can only be observed in experiments E4−E6, in which the added water exceeds 0.3 mL. However, the gels formed in the E4−E6 series are not as transparent as those prepared with nitric acid. It should be pointed out that when the nitric acid solution is replaced by a $NH_3{\cdot}H_2O$ or NaOH solution at the same concentration (F3 and F4, Table 1), the resultant gels become inhomogeneous phases in which flocculates can be observed, although they also form instantaneously.

Finally, to check the novelty of the current approach, two extra experiments (G1 and G2, Table 1) were performed using $Al(NO_3)_3{\cdot}9H_2O$ instead of ASB. As expected, no gelation was observed, although $Al(NO_3)_3{\cdot}9H_2O$ dissolved readily in the solvents.

Formation of acac−Al Compounds. Figure 1 reports a FTIR investigation for the above sample series.

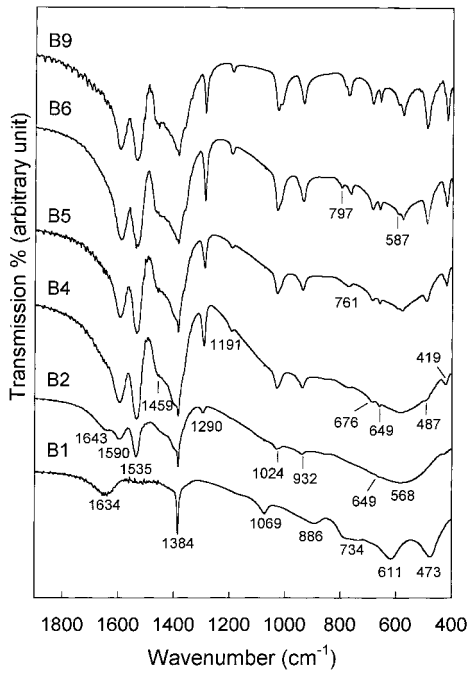

Figure 1. Representative FTIR spectra for sample series B1−B9 (uncalcined), noting that the acacH/ASB mole ratio = 0 (in B1) to 0.8 (in B9).

Indeed, substantial differences are observed between acac-chelated samples B2−B9 and the nonacac-chelated sample B1. Starting from B2, the peak intensities at 1590 and 1535 cm^{-1} are proportional to the amount of acacH added. These new peaks clearly indicate the chelation of the acetylacetonato groups to aluminum.[26−28] The vibrational mode of the $\nu C{=}O$ stretching (high frequency) of free acacH is not observed in the samples of B2−B9, which indicates a replacement of the O−*s*-Bu group by the acac.[26−28] In the vibrational region for Al−O−Al,[9] where Al is located in an octahedron formed by six oxygen atoms, the two well-defined peaks at 611 and 473 cm^{-1} have merged into one broad band (or become less defined) at approximately 568 cm^{-1} for the samples B2−B4. In agreement with the XRD findings, which will be presented shortly, the bending mode of the intercalated molecular water (in the boehmite or pseudoboehmite phase[29−31]) at 1634 cm^{-1} in the B1 sample is stronger than that of the water in the acac-chelated samples, which appears only as a shoulder (1643 cm^{-1}) in B2−B4. For the samples with higher acacH contents (B5−B9), stronger absorption peaks appear in the low-wavenumber region. These peaks are related mainly to the various organic functional groups of $Al(O\text{-}s\text{-}Bu)_{3-n}(acac)_n$ and trace organic compounds (including solvent and residual HO−*s*-Bu). Detailed assignments for these peaks can be found in Table

(26) Guertin, D. L.; Wiberley, S. E.; Bauer, W. H.; Goldenson, J. *J. Phys. Chem.* **1956**, *60*, 1018.
(27) Nakamoto, K. *Infrared Spectra of Inorganic and Coordination Compounds*; John Wiley and Sons: New York, 1962; p 216; *Infrared and Raman Spectra of Inorganic and Coordination Compounds*; John Wiley and Sons: New York, 1986; p 259.
(28) Leaustic, A.; Babonneau, F.; Livage, J. *Chem. Mater.* **1989**, *1*, 240.
(29) Maeda, K.; Mizukami, F.; Niwa, S.-I.; Toba, M.; Watanabe, M.; Masuda, K. *J. Chem. Soc., Faraday Trans.* **1992**, *88*, 97.
(30) Bagwell, R. B.; Messing, G. L. *Key Eng. Mater.* **1996**, *115*, 45.
(31) Ouyang, D.; Mo, C.; Zhang, L. *Nanostruct. Mater.* **1996**, *7*, 573.

Table 2. Observed IR Wavenumbers for Formation of Al^{III} Acetylacetonate Derivatives [$Al(O-s\text{-}Bu)_{3-n}(acac)_n$] and Their Assignments[a]

wavenumber (cm^{-1})	predominant modes
1590	$\nu(C-C) + \nu(C-O)$
1535	$\nu(C-O) + \nu(C-C)$
1459	$\delta(C-H) + \nu(C-C)$
1375	$\delta_s(CH_3)$
1290	$\nu(C-CH_3) + \nu(C-C)$
1191	$\delta(C-H) + \nu(C-CH_3)$
1024	$\rho_r(CH_3)$
932	$\nu(C-C) + \nu(C-O)$
797, 761	$\pi(C-H)$
676, 649	$\pi(CH_3-CO-C)$
587	ring deformation + $\nu(Al-O)$
487	$\nu(Al-O) + \nu(C-CH_3)$

[a] Symbols: ν, stretching vibration; δ, in-plane bending or deformation; δ_d, degenerate mode of deformation; δ_s, symmetric mode of deformation; ρ_r, rocking mode; π, out-of-plane bending.

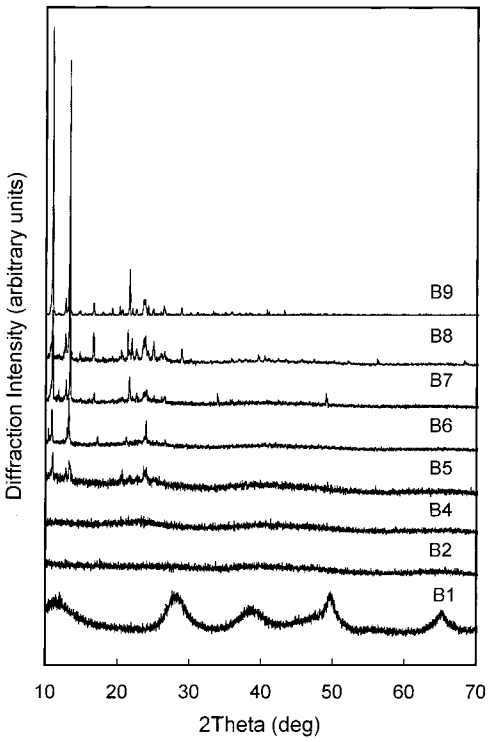

Figure 2. XRD patterns for sample series B1−B9 (uncalcined), noting that the acacH/ASB mole ratio = 0 (in B1) to 0.8 (in B9). The XRD patterns in B5−B9 are similar to those for $Al(acac)_3$.

2.[26−28] Figure 2 displays a set of XRD patterns measured for the sample series B1−B9 (Table 1). As can be seen, the B1 gel prepared without using acacH is basically in the boehmite or pseudoboehmite phase.[29−31] The average size of the crystallites in B1 is about 3 nm (determined from the Scherrer method using the $2\theta = 28°$ peak, Figure 2). When the mole ratio of acacH/ASB equals 0.1−0.3, the gel samples obtained (B2−B4) are amorphous. Crystallites formed in the gel phase can be observed for acacH/ASB ratios ≥ 0.4 (B5−B7). As mentioned earlier, no gelation is observed for the sols of B8 and B9, in which needle-like crystals can be observed. In fact, the XRD patterns of B8 and B9 represent a well-crystallized aluminum acetylacetonate $Al(acac)_3$ [or $Al(C_5H_7O_2)_3$].[32] Comparing the XRD patterns of the gel samples B5−B7 with those of B8 and B9, it can be concluded that aluminum acetylacetonate $Al(acac)_3$ is also formed in these samples, although the formation of other derivatives such as $Al(O-s\text{-}Bu)_{3-n}(acac)_n$ ($n = 1-3$) cannot be ruled out.[26−28]

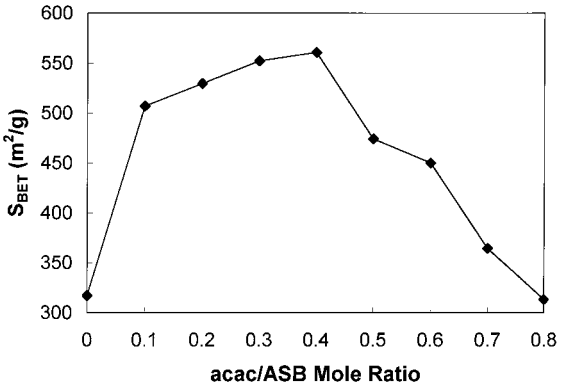

Figure 3. Specific surface area (S_{BET}) profile versus mole ratio acacH/ASB for the sample series B1−B9 after calcination at 400 °C for 2 h.

Table 3. Specific Surface Areas, Pore Volumes, and Pore Diameters Measured for Some Representative Samples after 2 h Thermal Treatments

sample	temp (°C)	S_{BET} (m^2/g)	pore vol (mL/g)	pore diameter (Å)
A2	200	538.0		
A3	200	554.1		
A6	200	559.0		
B1	400	317.0		
B2	400	507.3		
B3	400	529.6		
B4	400	552.1		
B5	400	560.6		
B6	400	474.6		
B7	400	450.4		
B8	400	364.6		
B9	400	313.2		
F1	400	400.0		
F2	400	402.5		
B4	(as prepared)	243.7	0.147	
B4	200	549.9	0.275	<16
B4	300	674.4	0.351	<16
B4	400	542.2	0.328	28.9
B4	500	313.8	0.271	33.8
B4	600	318.4	0.272	31.4
B4	800	233.6	0.178	35.2
B4	1000	55.4	0.103	74.1
B4	1200	1.4	0.007	

Specific Surface Area and acacH Content. Table 3 lists some representative S_{BET} data from the present study. It is found that the S_{BET} values of A2, A3, and A6 (calcined at 200 °C) are not solvent dependent, even though the gelation time for the sample A6 is much longer than those for A2 and A3. Figure 3 shows a S_{BET} profile for the samples B1−B9 (Tables 1 and 3) calcined at 400 °C. A sharp increase in S_{BET} (317 m^2/g for B1 to 507 m^2/g for B2) is observed when the acacH is used in the synthesis. It is observed that there is a maximum S_{BET} located at the mole ratio of acacH/ASB = 0.3−0.4, after which the S_{BET} decreases abruptly. This observation indicates that the use of acacH is advantageous to gain a larger surface area but too much of it causes a negative effect, that is, reduction of S_{BET}.

When the nitric acid is switched to a base, a relatively high S_{BET} can still be achieved, as shown by the data

(32) Powder Diffraction File, Card No. 42-1746. Joint Committee on Powder Diffraction Standards, Swarthmore, PA, 1995.

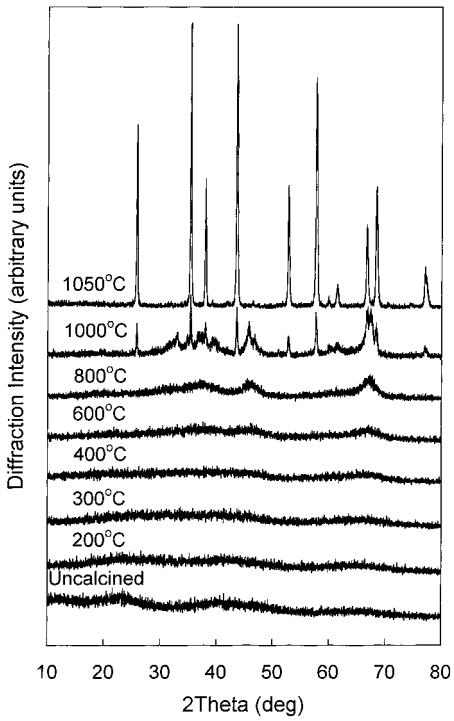

Figure 4. XRD patterns for the B4 sample (uncalcined and calcined at 200−1050 °C for 2 h), noting that in this sample the acacH/ASB mole ratio = 0.3.

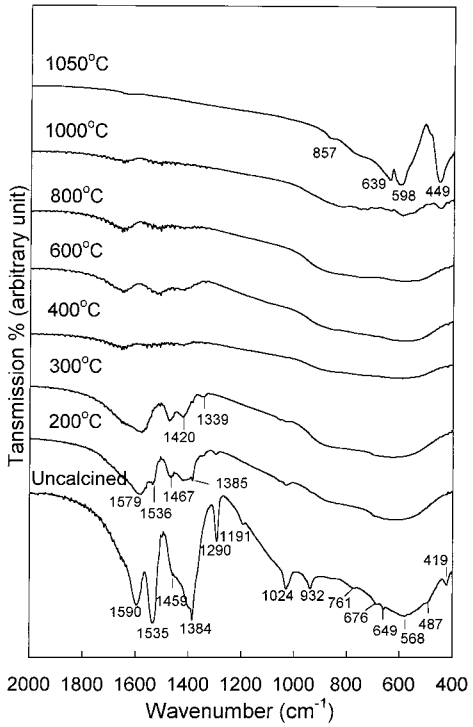

Figure 5. FTIR spectra for the B4 sample (uncalcined and calcined at 200−1050 °C for 2 h), noting that in this sample the acacH/ASB mole ratio = 0.3.

for F1 and F2 (400 and 403 m^2/g, Table 3). Basically, no difference in S_{BET} is observed for either $NH_3 \cdot H_2O$ or NaOH solution, although both of them reduce the transparency of the gels. Although the S_{BET}s of F1 and F2 are not as large as those of B2−B5, they are still larger than that of B1. This observation can be attributed to the usage of acacH in synthesis. It is recognized that introducing chelating agent acacH to the synthesis is crucial to increasing S_{BET}, whereas the selection of a proper hydrolysis catalyst is not as important.

Surface Area Change and Thermal Treatments. On the basis of the above results, it is apparent that the B4 or B5 sample can give a high surface area after calcination. In particular, the results from the B4 sample calcined at various temperatures (see Table 3) show a maximum S_{BET} (674 m^2/g) at 300 °C, and the S_{BET} decreases rapidly toward a compact nonporous phase when the temperature exceeds 800 °C.

To explain the above S_{BET} observations, Figure 4 displays a set of XRD patterns measured from the calcined B4 in the temperature range 200−1200 °C. As reported earlier, the dry as-prepared gel of B4 is amorphous, and this physical state remains throughout the range 200−400 °C. At 400−500 °C, the γ-Al_2O_3 pattern starts to emerge, and it becomes more apparent at 600−800 °C.[12] With a higher calcination temperature at 1000 °C, the α-Al_2O_3 pattern appears, and it fully develops at 1050 °C.[12] In agreement with the XRD results, the FTIR spectra shown in Figure 5 also indicate a similar structural evolution. For example, the functional groups of the organic components persist until calcination at 400 °C. The signature IR vibrations of γ-Al_2O_3 appear at 400 °C and develop fully at 800 °C.[33] The γ- to α-transition starts at 1000 °C and is completed at 1050 °C, as evidenced in the IR vibrational

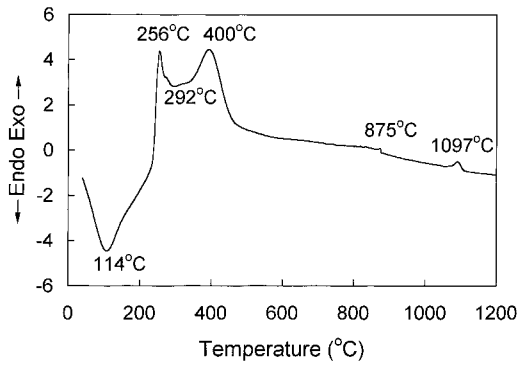

Figure 6. DTA scan for the A4 sample from room temperature to 1200 °C (in air, at 10 °C/min), noting that the chemical composition of A4 is between those of B4 and B5 (A4, acacH/ASB = 0.35; B4, acacH/ASB = 0.30; B5, acacH/ASB = 0.40; Table 1).

modes of α-Al_2O_3.[33] In connection with the above structural evolution, the thermal events occurring for sample A4 (its composition is between B4 and B5) upon the heat treatment were investigated with DTA/TGA, and the DTA results are shown in Figure 6. In the low-temperature region, a large endothermic peak is located at 114 °C, which can be assigned to evaporation and/or desorption of encapsulated water from condensation, solvent, and organic compounds, resulting from the gelation reactions of ASB. The two exothermic peaks at 256 and 400 °C can be attributed to the oxidative combustion and decomposition of the organic compounds (solvent and resultant ROHs) and the chelating agent acac, respectively, in view of the significant reductions in the IR peak intensities of acac at 200 and 400 °C (Figure 5). On the basis of XRD and FTIR results, a

(33) Gadsden, J. A. *Infrared spectra of minerals and related inorganic compounds*; Butterworths: London, 1975; p 43.

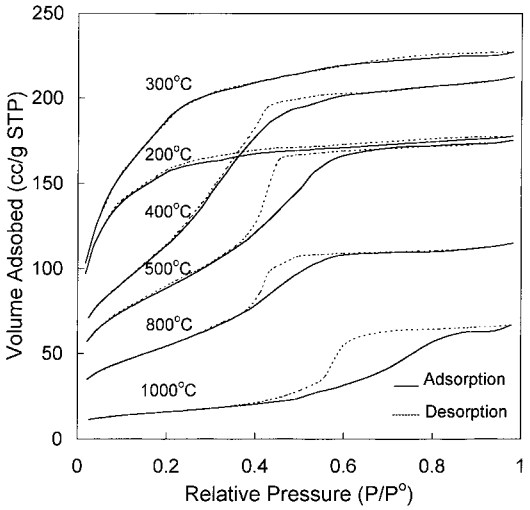

Figure 7. Representative nitrogen adsorption−desorption isotherms measured for B4 samples calcined at 200−1000 °C for 2 h.

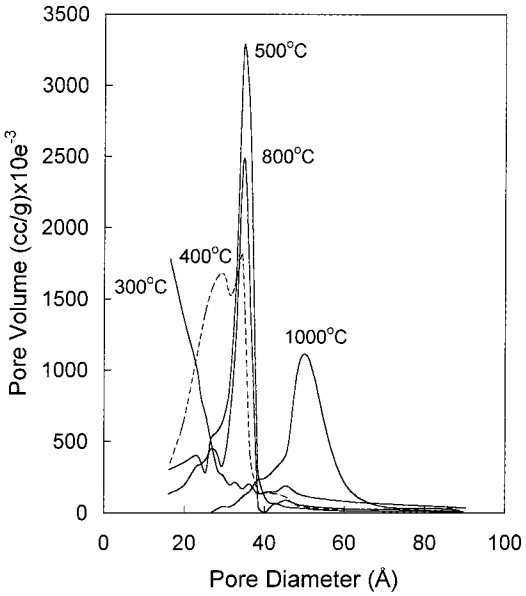

Figure 8. Representative pore size distribution profiles (BJH method) measured for the B4 samples calcined at 300−1000 °C for 2 h.

broad exothermic band at approximately 875 °C and a small exothermic peak at 1097 °C can be assigned to the formation of γ-Al_2O_3 and its transformation to α-Al_2O_3, respectively.[34]

Pore Size Distribution with Thermal Treatments. In Figure 7, adsorption−desorption plots are displayed for the calcined samples from B4 (Table 3). As shown, the adsorption−desorption curves overlap if the gel calcination temperature is below 300 °C. In these curves, there are two slopes that divide at $P/P° \approx 0.3$. Therefore, the adsorption−desorption data measured for these low-temperature calcined samples are typical Langmuir isotherms (type I).[35,36] It is also noted that higher N_2 uptake (adsorbed N_2 gas volume) is observed in the 300 °C calcined sample, compared to the 200 °C calcined sample, which can be explained by the S_{BET} variation between the two samples (Table 3).

When the calcination temperature is above 400 °C, the resultant adsorption−desorption data are quite different (400−1000 °C, Table 3). These curves can be assigned to the type IV isotherms for mesoporous materials.[35,36] First, compared with the case of the low-temperature calcined samples, the initial amount of adsorbed N_2 volume is much lower. Second, the adsorption and desorption curves begin to separate when $P/P° \approx 0.4$. The formation of hysteresis loops is due to capillary condensation in mesoporous materials. Third, with a further increase in $P/P°$, the capillary condensation ends and the two curves overlap again. Last, the total volume of adsorbed N_2 decreases with an increase of calcination temperatures over 400−1000 °C.

The very flat part of the curves in the high $P/P°$ region is indicative of a narrow pore distribution in these porous materials. Due to the instrumental limitations, it is not possible to determine the sizes for the two low-temperature calcined samples (200−300 °C; they are < 16 Å), as shown in Figure 8. For the 400−1000 °C calcined samples, indeed, a very narrow PSD is observed. Among them, the 500 °C calcined sample has the most uniform porosity. The general trend observed is that the PSD shifts toward larger pore radii with an increase in the heat-treatment temperature.

Discussion

Overview of the Synthesis. It has been recognized that the role of chelating agents is crucial in preparation of sol−gel-derived alumina materials. Using various chelating agents and sol−gel routes, as reported in the literature,[10−20] high-surface-area alumina materials have been synthesized. However, the formation mechanisms differ. For example, acetic acid and other carboxylic acids have been used in the synthesis of aluminum oxides.[15−17] It is found that when the mole ratio of CH_3COOH/ASB is ≥2, the gels produced are transparent and higher surface area and higher pore volume can be achieved.[15,16] These results can be attributed to the presence of unreacted acetate and OH ligands, which favors intramolecular condensation reactions during drying.[15,16]

A comparative study has been reported on chelating agents of acetylacetone (acacH) and ethyl acetoacetate (eaa) in the sol−gel synthesis of alumina.[11] It is found that, for acacH/ASB = 0.25−1.0, precipitates are formed after hydrolysis and translucent gels (acacH/ASB = 0.25) can be obtained even with a later addition of nitric acid (which was a peptization agent in that work). It is thus concluded that the stabilization effect of acacH is poorer than that of eaa.[11]

It should be mentioned that the addition of water and nitric acid in the present work was carried out in a single step, whereas in the previously reported work nitric acid (which was a peptization agent rather than a catalyst in the current work) was added only after hydrolysis and condensation There were also variations in the compositions of the precursors for the current work compared to previous works.[11] Compared to the

(34) Harizanov, O. A.; Surtchev, M. *Mater. Lett.* **1997**, *32*, 25.
(35) Astier, M.; Sing, K. S. W. *J. Chem. Technol. Biotechnol.* **1980**, *30*, 691.
(36) Sing, K. S. W.; Everett, D. H.; Haul, R. A. W.; Moscou, L.; Pierotti, R. A.; Rouquerol, J.; Siemieniewska, T. *Pure Appl. Chem.* **1985**, *57*, 603.

above investigations, the present synthesis study proposes a new type of precursor system and synthetic route for alumina synthesis. Unlike the case for the eaa or long-chain carboxylic acids,[11,17] the surfactant effect of the chelating agent in the present study can be largely ignored, as the molecular size of acacH and the mole ratio of acacH/ASB adopted are relatively small. As shown in the samples E1−E6, the gels prepared using water are not as transparent as those using nitric acid solution (Table 1). The improvement in gel transparency can be attributed to proper reaction rates of hydrolysis and condensation controlled by the nitric acid.

Mole Ratios of acacH/ASB in Precursor Solutions. It is noted that gel formation occurs in samples B2−B5 but not in the B6−B9 samples. On the basis of the FTIR study (Figure 2), the formation of acac−Al complexes in B2−B5 has been confirmed, although the samples B2−B5 are largely amorphous. Since transparent gels are obtained in B4 and B5 (see Results), which indicates the chelating effect of acac on control of the hydrolysis and condensation rates, the mole ratio acacH/ASB = 0.3−0.4 can be considered to be optimal for this precursor system. It is known that the acetylacetonato ligand is able to bridge metal cations (μ-bonding) although it is not the favored process in general.[37,38] Since the acacH/ASB mole ratio in these two samples is low, it is believed that not all ASB molecules are bound to the chelating agent. All stretching/bending modes reported in the Results indicate the formation of a planar chelate ring structure and the presence of resonance in the chelate ring.[26−28] These results in turn suggest the following reaction, which leads to the formation of singly acac-chelated ASB (i.e., monoacetylacetonato−Al alkoxide) before hydrolysis takes place:[11]

$$\mathrm{Al(O{-}\textit{s}\text{-}Bu)_3 + acacH \rightarrow Al(O{-}\textit{s}\text{-}Bu)_2(acac) + HO{-}\textit{s}\text{-}Bu} \quad (1)$$

It has been known that there are several structures for monoacetylacetonato−Al alkoxides, which give rise to four-, five-, and six-coordinated Al atoms.[10] For example, the trimeric $Al(OR)_2(acac)$ species has long been known.[38]

Gelation Rate and Precursor Composition. On the basis of the synthetic results, it is clear that the gelation rate can be decreased with the chelating agent acacH. As discussed above, due to the formation of acac-chelated species, the overall reactivity of ASB toward water has been reduced; that is, fewer free ASB molecules are present in the solutions.

Regarding the gelation rate in different sols, several chemical processes, such as hydrolysis and polycondensation, need to be further considered.[15−17] In the present study, the hydrolysis process has been investigated by varying the water content while keeping the other preparation parameters unaltered. As revealed in the sample series of D1−D5 and E1−E6 (Table 1), the gelation rate increases with an increase in the water content. In particular, a significant increase in the gelation rate is observed for the cases of mole ratio H_2O/ASB > 2 in both sample series (i.e., the amount of water ≥ 0.4 mL, D2−D5 and E4−E6, Table 1). Considering the hydrolysis reactions of ASB and $Al(O{-}\textit{s}\text{-}Bu)_2(acac)$ below

$$\mathrm{Al(O{-}\textit{s}\text{-}Bu)_2(acac) + 2H_2O \rightarrow Al(OH)_2(acac) + 2HO{-}\textit{s}\text{-}Bu} \quad (2)$$

$$\mathrm{Al(O{-}\textit{s}\text{-}Bu)_3 + 3H_2O \rightarrow Al(OH)_3 + 3HO{-}\textit{s}\text{-}Bu} \quad (3)$$

it is recognized that the stoichiometric mole ratio of H_2O/ASB should be >2, which is indeed observed in the present work. As polycondensation generates water molecules, the observed mole ratio H_2O/ASB > 2 would suggest that the hydrolysis is completed before the polycondensation. Therefore, it seems the hydrolysis is a controlling step in the overall gelation process.

When D1−D5 samples were compared with E1−E6 samples, the only difference found was the degree of transparency of the resultant gels. The nitric acid used in D1−D5 can be thought to have dual functions. On one hand, it provides a water source (as in E1−E6) for hydrolysis, and on the other hand, it acts as a catalyst or an acidification agent for acac. In general, gels with good transparency can be prepared with a fairly wide range of the acid molarity, as revealed in the samples C1−C8 (Table 1). When the acid molarity exceeds 1.2 M, the gels prepared (C9 and C10) are opaque and their gelation times are very short. This observation can be attributed to the acidification effect of acac (to form acacH), which frees the acac from the cheleated ASB and thus increases the hydrolysis rate of ASB.

Changes of S_{BET} and PSD with Structural Evolution. Although water and nitric acid affect the gelation rate and gel transparency significantly, their effects on the S_{BET} and PSD values are not as pronounced. As reported in Table 3 and Figures 3, 7, and 8, the S_{BET} and PSD values of each sample depend heavily on its acacH content and the thermal treatment received.

The effect of acacH on S_{BET} can be related to the formation of a suitable gel structure from which a high-surface-area gel can be generated after calcination. Figure 3 indicates that the acacH content must be controlled in the range acacH/ASB = 0.3−0.4, since it controls the chemical content and the microstructure of the gels. When a suitable acacH content is found, selection of a proper heating temperature is further needed to carefully control the chemical reactions. It should be pointed out that, in addition to these chemical reactions, temperature-dependent phase transformation also plays an important role in the morphological/textual development of the gels.

Although the gel reactions and phase transformation are closely coupled in the low-temperature region, the phase transformation can be considered as a dominant process after approximately 500 °C (Figure 6), since thermal events for the latter are generally less noticeable and no further weight loss is detected by TGA. For example, at 300 °C (noting that after the first exothermic event, Figure 6), the peak intensities for organic functional groups in the B4 sample (with high S_{BET} = 674 m^2/g) are getting weaker but they are still detectable in the IR spectrum (300 °C, Figure 5). Because it is heat-treated only at 300 °C (before the second exothermic event, Figure 6) and the XRD (Figure 4) gives no diffraction pattern, the high-S_{BET} sample B4 is in fact a half-reacted amorphous gel. Over the

(37) Ribot, F.; Toledano, P.; Sanchez, C. *Chem. Mater.* **1991**, *3*, 759.
(38) Mehrotra, R. C.; Rai, A. K. *Polyhedron* **1991**, *10*, 1967.

temperature range 200−300 °C, the S_{BET} value increases. Two successive declines in S_{BET} are observed at 400 and 1000 °C (Table 3) respectively, at which the γ-Al_2O_3 and α-Al_2O_3 phases become recognizable. Unlike the chemical reactions that generate higher surface areas at 200−300 °C (Table 3), the phase transformation at high temperature causes a sequential reduction in S_{BET}. While the pore volume data show a similar trend to that for the S_{BET} values (i.e., small-to-large-to-small, Table 3), the PSD data show an increasing enlargement in pore size (i.e., small-to-large). Interestingly, it is noted that the pores in the heated gels were almost doubled in size after each phase transformation (amorphous → γ ··· → α). Therefore, on the basis of this PSD evolution, alumina powders with a tuneable pore size can be prepared by selecting a proper heat-treatment temperature.

Possible Mechanisms for High Surface Area and Pore Formation. The formation of the boehmite phase can be described by the following reaction after the formation of aluminum trihydroxides:[39]

$$Al(OH)_3 \rightarrow AlO(OH) + H_2O \quad (4)$$

Judging from the diffraction pattern and peak width, it is known that the xerogel prepared without using acacH is indeed in the boehmite phase (B1, Figure 1) and the particle size is small, as unchelated ASB will result in $Al(OH)_3$ after hydrolysis. Nonetheless, the boehmite XRD pattern is not observed in the samples prepared with a small amount of acacH molecules (B2−B4, acacH/ASB = 0.1−0.3). Instead of producing $Al(OH)_3$, the acac-chelated ASB gives rise to $Al(OH)_2$(acac) after hydrolysis reaction 2, which is then followed by the condensation reaction below:

$$2Al(OH)_2(acac) \rightarrow (acac)(HO)Al{-}O{-}Al(OH)(acac) + H_2O \quad (5)$$

For the samples B2−B4, only 10−30 mol % of the ASB molecules is in the form of $Al(OH)_2$(acac) while 90−70 mol % of the ASB is $Al(OH)_3$, on the basis of reactions 2 and 3. It is likely that intermolecular polycondensation reactions between these hydroxides, which form various oxo species, will lead to the amorphous state observed in the B2−B4 gels. As explained schematically in Figure 9, since the concentration of acac is small, there are many possible locations for an acac in replacing an OH group within the boehmite-like structure. Due to the random distribution of acac and the steric effect (bulkiness) of the molecule, which will enlarge the intersheet spacing, a defective and distorted structure results.

It has been known that the microporosity of the boehmite or pseudoboehmite phase is created by the packing of crystallites and there is no addition of intracrystalline porosity during the thermal decomposition of the boehmite or pseudoboehmite phase at 450 °C.[27,39] In contrast, the porosity development during the serial heating of the B4 sample shows some pore volume gains in association with the S_{BET} rises at 300−400 °C

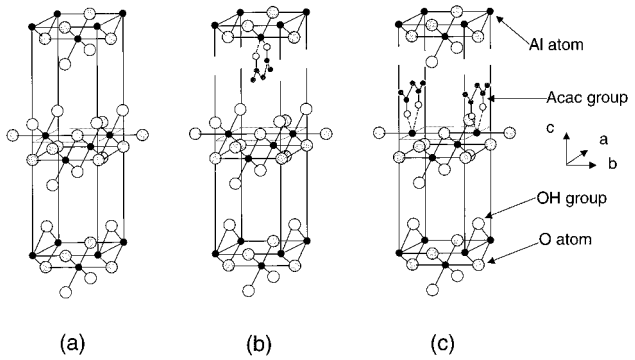

Figure 9. Possible mechanisms for transformation from the boehmite phase (B1) to the amorphous state (B2−B5): (a) unit cell of boehmite structure; (b) acac group in replacement of an OH group within the boehmite-like structure with acac/Al mole ratio = 1:4; (c) same as in part b but with an opposite orientation for acac groups (acac/Al mole ratio = 1:4); discontinued vertical lines indicate an expansion of the intersheet spacing.

(Table 3). This observation can be attributed to the chemical modification of acac. As evidenced in Figure 5, the IR peaks of acac−Al are weakened in this temperature range (300−400 °C). In agreement with the IR observation, the DTA scan (in air) of Figure 6 reveals a small endothermic dip at approximately 292 °C, which can be ascribed to the thermal detachment of acac, and a large exothermic band at 400 °C, which can be assigned to the oxidative decomposition of acac. Because these chemical reactions occur at the molecular level, it is our belief that the gains in S_{BET} and pore volume upon thermal treatment are due to the development of intraparticle porosity.[27,39]

At higher temperatures (500−1200 °C), the porosity data in Table 3 can be attributed to the packing of agglomerates of decomposed hydroxides and oxides. Processes such as dehydration (started at 450 °C),[27,39] phase transformation, and particle growth upon heat treatment become important in this temperature range, and they will result in larger pore sizes and smaller S_{BET} values due to the size and density changes of the particles.[40]

Conclusions

In summary, transparent alumina gels can be prepared with optimal acacH/ASB mole ratios of 0.3−0.4 using the present precursor system. High S_{BET}s of 552−560 m^2/g have been obtained for these gels after calcination at 400 °C (2 h), due to the formation of acac−Al compounds in the precursor sols. It is found that the amorphous gels convert into γ-Al_2O_3 at 400−800 °C and later to α-Al_2O_3 at 1000−1050 °C. In response to the two phase transformations, two successive declines in S_{BET} are observed at 400 and 1000 °C, respectively. Microporous alumina (pore size < 16 Å) can be prepared at the calcination temperatures 200−300 °C (S_{BET} = 674 m^2/g) while mesoporous samples (pore size = 29−74 Å) can be obtained at 400−1000 °C using the same starting xerogel. On the basis of a large set of gelation data, it is believed that the hydrolysis of alkoxides takes place

(39) Poisson, R.; Brunelle, J.-P.; Nortier, P. In *Catalyst Supports and Supported Catalysts: Theoretical and Applied Concepts*; Stiles, A. B., Ed.; Butterworths: Boston, 1987; Chapter 2, p 11.

(40) Vendange, V.; Colomban, Ph. *J. Mater. Res.* **1996**, *11*, 518.

before the condensation. The improvement in gel transparency can be attributed to the new synthesis process and the optimal precursor composition proposed in this work, and the high surface areas observed in the low-temperature heated samples can be ascribed to an acacH modification of the boehmite-like structure which creates intraparticle porosity upon thermal treatment.

Acknowledgment. The authors gratefully acknowledge research funding (RP960716 and A/C50384) co-supported by the Ministry of Education and the National Science and Technology Board of Singapore. L.J. wishes to thank the National University of Singapore for providing a postgraduate scholarship.
CM990404U